HiSST: International Conference on
High-Speed Vehicle Science Technology
26–29 November 2018, Moscow, Russia

Starting and heating of rectangular hypersonic inlet with blunted leading edges

V. Borovoy[1], V. Mosharov[2], A. Skuratov[3] and V. Radchenko[4]

Abstract

Experimental investigation of the flow in a schematic rectangular air inlet mounted on a plate is carried out. The influence of leading edges bluntness and narrowing degree of the internal channel on the inlet starting and on the heat transfer inside it are studied. The experiments are carried out at two Mach numbers (M_∞=5 and 8) and different Reynolds numbers $Re_{\infty L}$ from 2.8×10^6 to 23×10^6.

Keywords: *air inlet, starting, heat transfer, entropy layer, Ludwieg wind tunnel*

Nomenclature

Latin
L – Plate length
M – Mach number
Re – Reynolds number
St – Stanton number
W– Inlet channel width
r_1, r_2, r_3 – Bluntness radii of the plate, cowl and wedges correspondingly
Greek
δ^* – Displacement thickness of the boundary layer
Δ, Δ^* – Thickness and displacement thickness of the high entropy layer
$\eta = W_0/W_t$ – Channel narrowing degree
Subscripts
0 – Related to the channel entrance
1, 2, 3 – Related to the plate, cowl and wedges
ef – Effective
s – Behind the normal shock
t – Related to the channel throat
∞ – Undisturbed flow parameter

1. Introduction

A lot of works has been devoted to the investigation of hypersonic air inlets (see for example [1-14]. Usually the air inlets with sharp leading edges were considered. At the same time, at high flight speeds, the leading edges of the inlet must have some bluntness to limit the surface temperature. However at hypersonic speeds, even a small blunting of the leading edges can have a great impact on the flow, because the blunted leading edge generates the high-entropy layer in which gas density is many times less than in the oncoming stream. In this paper (see also [15, 16]), the influence of slight bluntness of the leading edges on the inlet starting and the gas flow inside it is investigated.

In most works, the integral characteristics of the air inlet were studied. In the present paper, heat transfer and flow structure inside the inlet are studied in detail. Such an opportunity arose due to the use of the transparent walls of the experimental model and panoramic methods, developed by the authors.

2. Experimental model, flow characteristics and methods of investigation

Figure 1,*a* presents the experimental model. The inlet of the internal compression type is mounted on the plate *1*. The plate simulates an wing surface, on which the inlet is located under real conditions

[1] *Central Aerohydrodynamic Institute, Zhukovsky, Moscow Region, Russia. Volf.borovoy@tsagi.ru*
[2] *Central Aerohydrodynamic Institute, Zhukovsky, Moscow Region, Russia. vladimir.mosharov@tsagi.ru*
[3] *Central Aerohydrodynamic Institute, Zhukovsky, Moscow Region, Russia. skuratov.ark@yandex.ru*
[4] *Central Aerohydrodynamic Institute, Zhukovsky, Moscow Region, Russia. vrad@progtech.ru*

and on which the external air compression occurs (before entering the inlet). Above the wedges *2*, the cowl *3* is installed. The bluntness radii of the plate, wedges and cowl can be varied by means of replaceable details. Fig. 1,*b* shows shock waves and rarefaction waves calculated for the two-dimensional inviscid gas flow at $M_\infty = 5$.

The experiments were carried out in the wind tunnel of TsAGI UT-1M, operating in the Ludwieg tube mode. Measurements of heat transfer were performed using the thin luminescent paint sensitive to the temperature [17]. The surface flow is visualized by the oil marked by contrast fluorescent particles [18]. This method presents in addition visualization of shear stress distribution. In order to study the flow inside the inlet, a part of the cowl and one wedge were made of a material that is transparent both for the exciting ultraviolet light and for the visible fluorescent light.

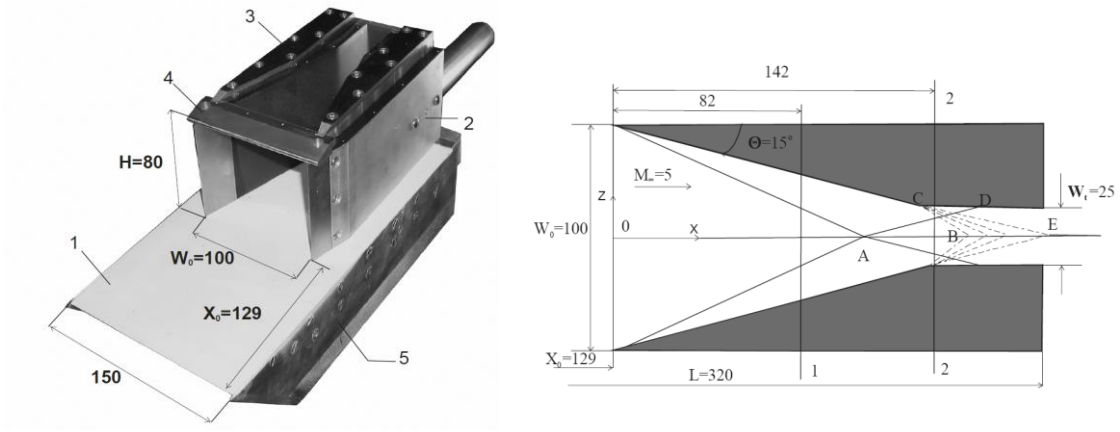

a *b*

Fig 1. Inlet model: *a* - model photo, *b* - cross section parallel to the plate. *1* - plate, *2* - wedges, *3* - cowl, *4* - replaceable leading edge of the cowl, *5* - side fences

3. Conditions of inlet starting

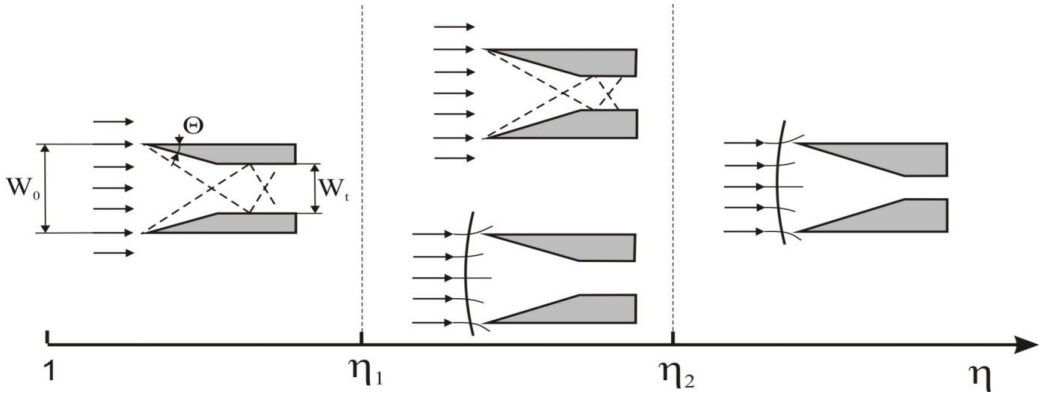

Fig 2. The ranges of the channel narrowing degree

The problem of inlet starting appears when the air inlet contains the narrowing channel. Considering the conditions of channel starting in the one-dimensional approximation with constant characteristics of the oncoming flow, it is possible to distinguish three ranges of the channel narrowing degree $\eta = W_0/W_t$ (Fig.2, W_t is the throat width).

1) For $\eta<\eta_1$, the channel always starts, and supersonic flow is formed inside it.

2) For $\eta_1<\eta<\eta_2$, two modes are possible: with supersonic velocities inside the channel (starting of the channel) and with subsonic velocities inside the channel (non-starting or blockage of the channel). In the second case, a bow shock wave forms ahead the entrance; behind the shock wave, a part of the incoming jet, corresponding to inlet width W_0, flows outward. At the unstart, the total pressure losses are much greater than when the channel is started. The implementation of a particular flow mode depends on the flow prehistory. In the short duration (impulse) wind tunnels, for example in the

Ludwieg type wind tunnel UT-1M, starting of the channel is more often realized. In the long duration wind tunnels, the channel is usually unstarted.

3) For $\eta > \eta_2$, the channel cannot be started and the flow with the detached bow shock wave is always realized.

The value of η_1 can be determined from the mass flow equation:

$$\rho_\infty U_\infty W_0 = \rho_* U_* W_t \tag{1}$$

$$\eta_1 = \rho_* U_* / \rho_\infty U_\infty \tag{2}$$

Here ρ_∞ and U_∞ are the gas density and velocity in the undisturbed flow, and ρ_* and U_* are analogous values in the channel throat. It is assumed that the normal shock wave is formed just before the entrance to the channel. Behind the normal shock, between the channel entrance and the throat, the compressed gas is isentropically accelerated to the sound velocity U_*, and its density drops to the corresponding value of ρ_*. Equation (1) implies the Kantrowitz relation [1]:

$$1/\eta_1 = [(\gamma - 1)/(\gamma + 1) + 2/(\gamma + 1)M_\infty^2]^{1/2}[2\gamma/(\gamma + 1) - (\gamma - 1)/(\gamma + 1)M_\infty^2]^{1/(\gamma-1)} \tag{3}$$

where $\gamma = C_p/C_v$ is the ratio of gas specific heats at constant pressure and constant volume.

The values of η_1 are small: for $M_\infty=5$ $\eta_1 = 1.54$, for $M_\infty=8$ $\eta_1=1.61$, and for $M_\infty=\infty$ $\eta_1=1.67$ ($\gamma = 1.4$). Accordingly, the gas compression ratio is also small. Therefore, it is of practical interest to realize supersonic flow in a channel with a large narrowing degree (for $\eta > \eta_1$).

In the absence of the bow shock wave, the maximum narrowing degree (η_2), at which supersonic flow in the channel is still possible, as in the presence of the bow shock wave, is limited by the flow capacity of the channel throat. It can be determined also by the equation (1). However, in this case, the gas density in the throat ρ_* must be determined using the gas density in the oncoming stream ρ_∞ taking into account the total pressure losses. They are due to the gas viscosity and presence the shock waves inside the channel. Blunting the leading edges of the wedges causes additional losses due to the formation of bow shock waves. In the particular case of isentropic flow in the channel, the values of η_2 are significant (as in the inverse Laval nozzle): for $M_\infty=5$ $\eta_2=25$, and for $M_\infty=8$ $\eta_2=190$. However, the total pressure losses in the shock waves significantly reduce the values of η_2: for the inviscid gas flow in the schematic inlet shown in Fig. 1,*b* for $M_\infty=5$ $\eta_2=14.7$, and for $M_\infty=8$ $\eta_2=51$. The gas viscosity and blunting of the leading edges significantly reduce the value of η_2.

The effect of the gas viscosity and wedge bluntness can be approximately taken into account by replacing the actual throat width W_t by the effective width $W_t - \delta^* - \Delta^*$, where δ^* and Δ^* are the displacement thicknesses of the boundary and entropy layers. Then for the coefficient of effective channel narrowing degree we obtain:

$$\eta_{ef} = \frac{\eta}{1 - \dfrac{2(\delta^* + \Delta^*)}{W_t}} \tag{4}$$

The coefficient of effective narrowing degree η_{ef} does not take into account losses in the internal shock waves. It also does not take into account the three-dimensional effects appearing when the shocks generated by the wedges interact with the boundary layer of the plate and cowl. These effects can have a great influence on the inlet flow at large distance between the inlet and the leading edge of the plate or the cowl. Therefore, the value of η_{ef} cannot serve as the only criterion for the inlet blockage. But it reflects the tendency of approaching the blockage or removing from it with a change in the wedge bluntness radius and the Reynolds number. The experimental data presented below show that at the wedges angle $\theta=15^0$, the inlet is blocked when η_{ef} approaches $\eta_{ef}=4.5$ at $M_\infty=5$ and $\eta_{ef}=4$ at $M_\infty=8$.

The thickness Δ and the displacement thickness Δ^* of the high entropy layer can be estimated using some assumptions presented in [16]:

$$\frac{\Delta}{r} = \frac{p_\infty}{p_e}\frac{T_\Delta}{T_\infty}\frac{U_\infty}{U_\Delta}\mathrm{Cos}\,\theta \tag{5}$$

Here θ is the slope of the wedge surface to the unperturbed flow direction, Δ is the thickness of the high entropy layer, and ρ_Δ, T_Δ and U_Δ are the gas density, temperature and velocity in the high entropy layer at a great distance from the wedge leading edge. These values are determined depending on the ratio P_e/P_s, where P_e is the pressure on the surface of the sharp wedge, and P_s is the total pressure behind the normal shock wave. For the displacement thickness of the high entropy layer, the following expression is obtained (the index e refers to the inviscid flow on the sharp wedge):

$$\frac{\Delta^*}{\Delta} = 1 - \frac{T_e}{T_\Delta}\frac{u_\Delta}{u_e} \tag{6}$$

From relation (5), it can be seen that with increasing wedge angle θ, the thickness of the high entropy layer decreases due to the increase in pressure P_e and the thickness of the compressed layer, which is deflected on the wedge inclined surface. For the wedge angle θ=15°, the following estimates are obtained: for M_∞=5 – Δ^*/r=0.6, and for M_∞=8 – Δ^*/r=0.8.

4. Flow patterns

The experimental data presented below show that one of the two flow patterns shown in Fig. 3 is realized in the inlet of the type considered.

If the channel is started, the regular flow with internal oblique shock waves and local separation zones is realized (Fig. 3,*a*). The wedge shocks generate narrow local separation zones. In them, the gas is involved in the longitudinal spiral flows along the undisturbed flow direction. Up to the intersection point of the wedge influence zones, the flow near each wedge does not differ from the flow near a single wedge. Behind this point, a more complex flow is formed, which was studied in detail in [20].

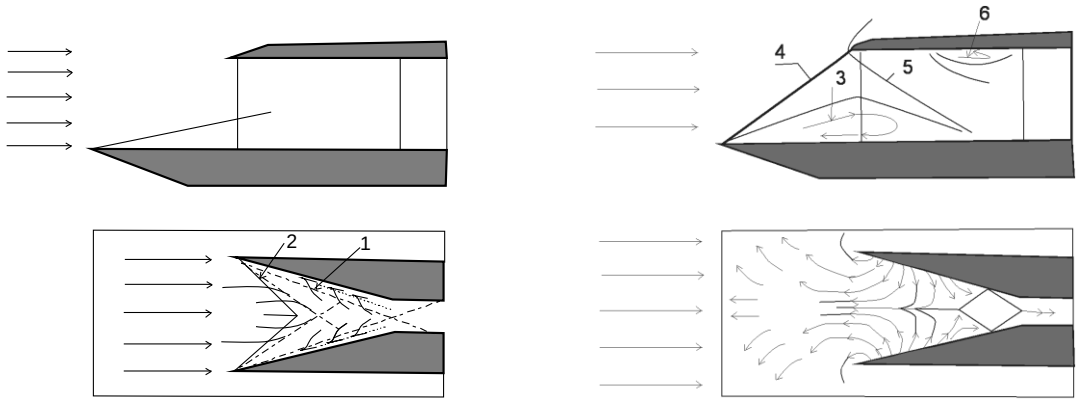

Fig 3. Flow patterns: *a* - regular flow, *b* - blockage of the inlet. *1* - the wedge shock, *2* – separation shock (separation line), *3* - global separation zone, *4* – shock of the global separation, *5* – bow shock wave of the cowl, *6* - separation zone on the cowl

For the blocked channel, the flow pattern is shown in Fig. 3,*b*. If the inlet were installed near the plate leading edge, the channel blockage would lead to the formation of a detached bow shock wave before it. Since the investigated inlet is installed at a considerable distance from the leading edge, the interaction of the shock wave with the plate boundary layer leads to the separation of the boundary layer in front of the inlet, the formation of the global separation zone and the separation shock (Fig. 3,*b*). The position of the separation line depends on the relative height of the inlet H/X_0.

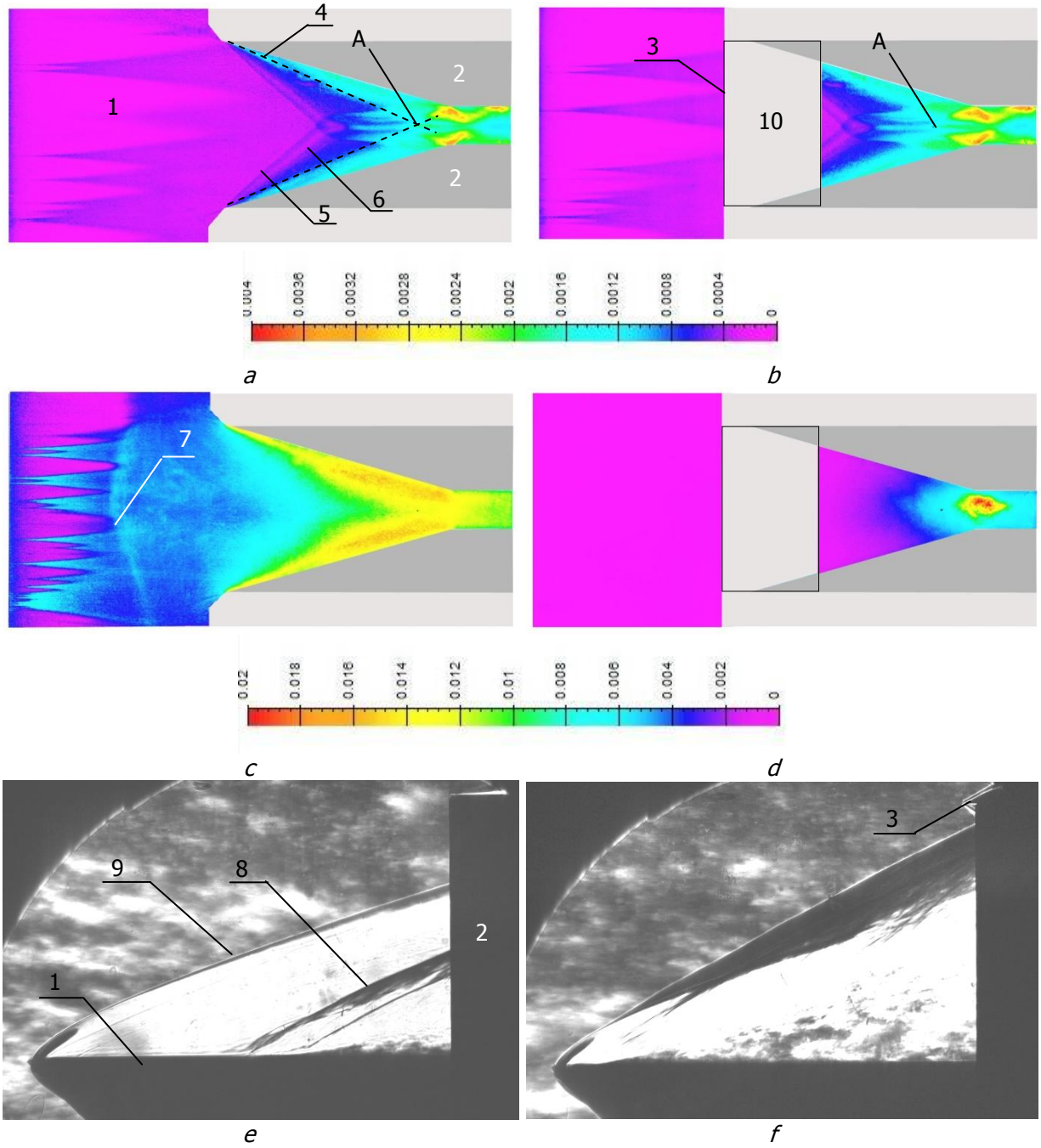

Fig 4. Distribution of the Stanton number over the plate surface and schlieren-photographs of the flow around the inlet model at M_∞=5, $Re_{\infty L}$=23×10^6 and η=4: on the left - in the absence of the cowl, on the right - in the presence of the cowl; *a, b* - the plate bluntness radius r_1=0.75 mm, *g, d, e, f* - r_1=2 mm; *1* - plate, *2* - wedges, *3* - cowl, *4* - wedge shock, *5* - boundary of the wedge-shock influence, *6* – local separation-line on the plate, *7* - global separation-line on the plate, *8* – shock of global separation, *9* – bow shock wave of the plate, *10* - opaque part of the cowl.

Fig 5. Effect of cowl presence on the flow between the wedges

The problem of the cowl influence is important because it is related to the influence of the inlet height on the gas flow. Figure 4 shows the flow around a pair of wedges at two values of the plate bluntness radius r_1. At r_1=0.75 mm (Fig.4,*a,b*), the channel blockage does not occur both in the absence of the cowl and in its presence: in both cases, the regular flow is established between the wedges. With the larger plate bluntness radius r_1=2 mm (Figure 4,*c*), the channel formed between the wedges is locked in both cases. The cowl presence influences the flow in different ways depending on the flow

structure: at the regular flow, the cowl practically has no effect on the flow; at the blockage of the channel, the cowl lengthens the separation zone because the cowl excludes the gas outflow from the inlet along the wedges.

In Fig. 5 the Stanton number distributions along the plate symmetry line Z = 0 are compared in the absence and in the presence of the cowl for two close values of the plate bluntness radius: r_1=0.75 mm and 1 mm (in the presence of the cowl, there are no data under the opaque section of the cowl X = 110-120 mm). Point O corresponds to the leading edges of the wedges. At r_1=0.75 mm, the regular flow is established. In this case, the Stanton number distribution is practically independent of the cowl presence (by the way, it should be noted that the cowl presence did not affect the measurement accuracy on the plate). At r_1=1 mm, the channel is locked. In this case, in the cowl presence, the maximum value of the Stanton number increases approximately 6-fold, and without the cowl, it changes insignificantly.

Thus, it can be concluded that, in the absence of blockage, the inlet height practically has no effect on the flow, if $H/W_o \geq 0.8$.

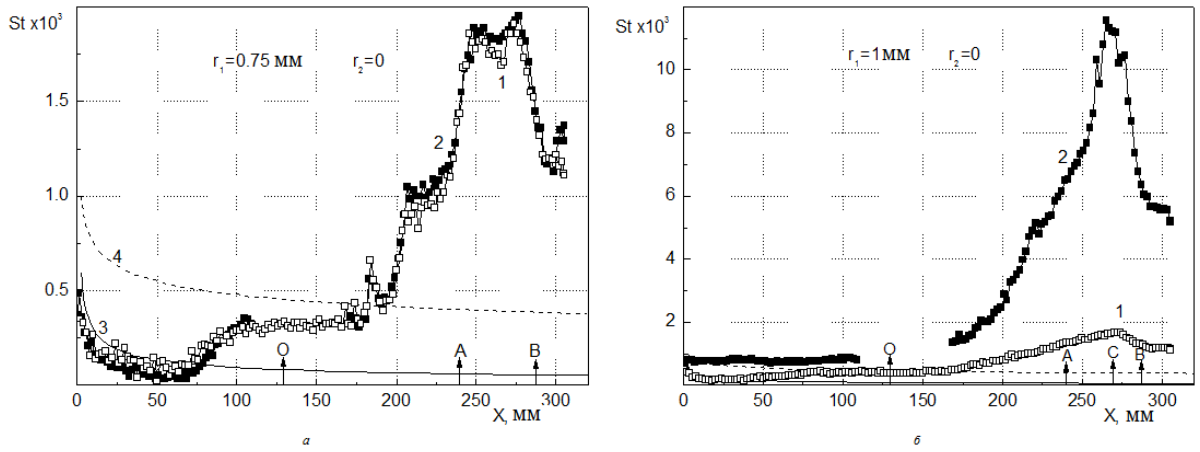

a *b*

Fig 6. The Stanton number distribution along the symmetry line Z = 0 at M_∞=5, $Re_{\infty L}=23\times10^6$ and η=4: *a* - the plate bluntness radius r_1=0.75 mm, *b* - r_1=1 mm; *1* - without cowl, *2* - with sharp cowl, experiment; *3* - laminar boundary layer, *4* - turbulent boundary layer, calculation.

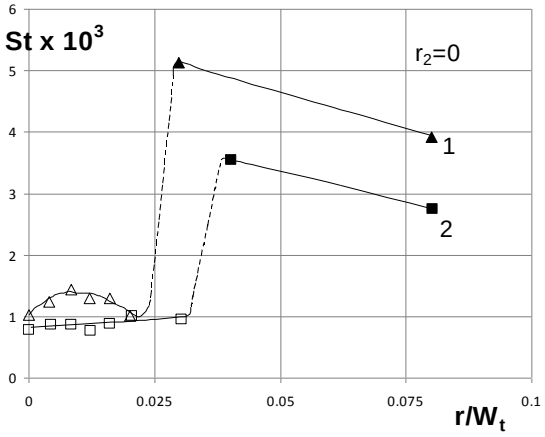

Fig 7. Influence of plate bluntness on heat transfer on the plate surface in the cross section 1 at M_∞=5 and η=4: *1* - $Re_{\infty L}=13\times10^6$, *2* - $Re_{\infty L}=23\times10^6$.

5. Influence of inlet geometrical characteristics and oncoming-flow parameters on the gas flow and heat transfer

5.1. Plate bluntness radius r_1

Fig. 6 shows the Stanton number values on the plate symmetry line Z = 0 in section 1, which is located in front of the inlet throat (see Figure 1,*b*), in dependence on the plate bluntness radius r_1. The sharp increase of Stanton number indicates the channel blockage. Decrease of Reynolds number causes a decrease in the plate bluntness radius, causing the inlet blockage: for $Re_{\infty L}=23\times10^6$ the blockage occurs when $r_1/W_t\approx0.032$ ($r_1\approx0.8$ mm), and for $Re_{\infty L}=13\times10^6$ this occurs when $r_1/W_t\approx0.026$ ($r_1\approx0.65$ mm). The corresponding values of the effective coefficient of the channel narrowing degree η_{ef} were calculated using the relation (4). It was assumed that in both cases the plate boundary layer is turbulent. For the two cases mentioned above, the same value of η_{ef} at the channel blockage is obtained: η_{ef} = 4.65.

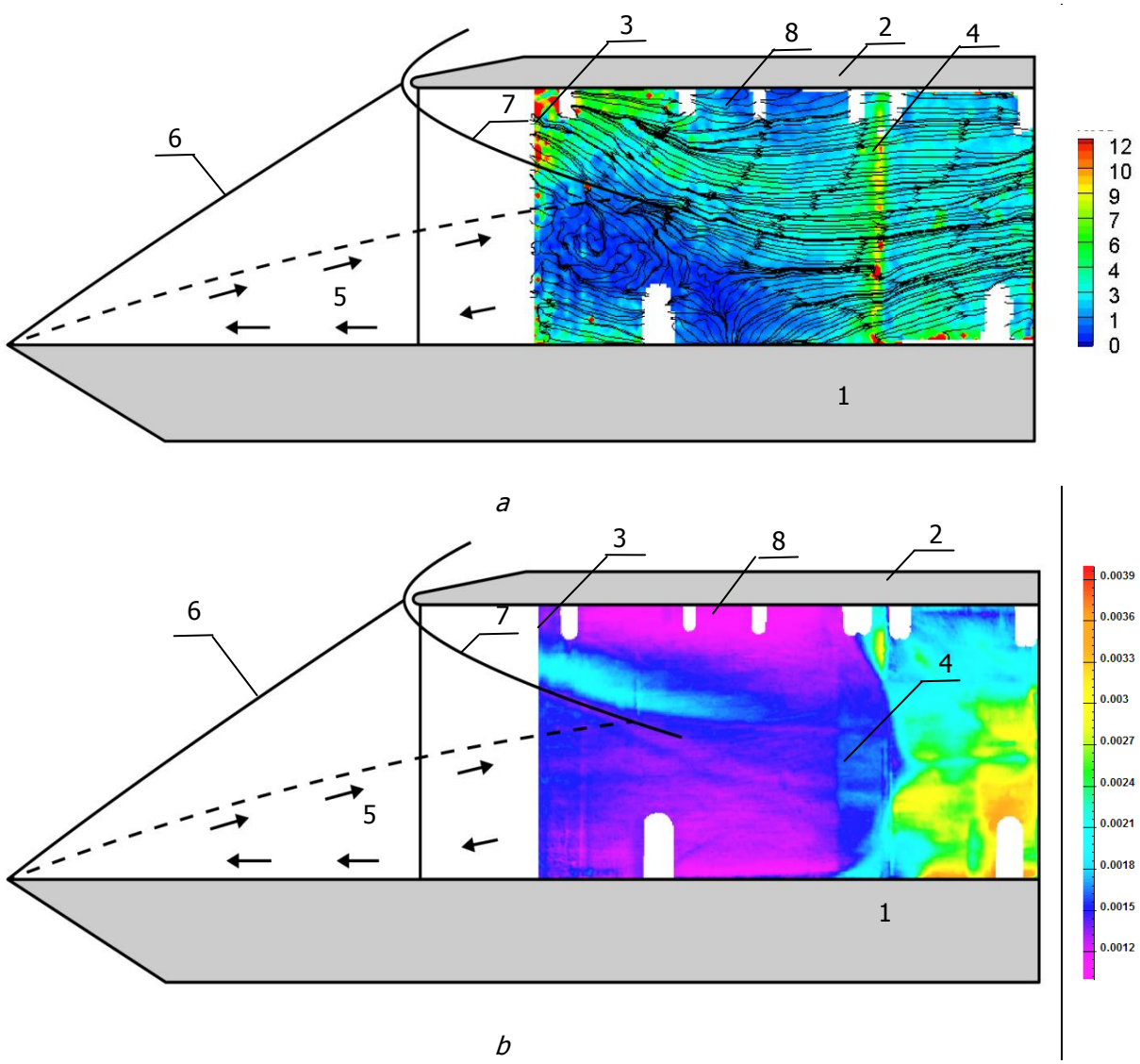

Fig 8. Flow structure and heat exchange on the wedges in the inlet with blunted cowl (r_2=2 mm) at M_∞=5 and $Re_{\infty L}=23\times10^6$: *a* - visualization of surface stream lines and shear stresses, *b* - Stanton number distribution; *1* - plate, *2* - cowl, *3* - wedge, *4* - edge of wedge, *5* – separation zone on the plate, *6* – separation shock, *7* - bow shock wave of the cowl, *8* - separation zone on the cowl.

5.2. Cowl bluntness radius r_2

At sufficiently large cowl bluntness, global separation zone is formed and the inlet is locked, as at large plate bluntness. The reasons for this phenomenon are discussed below.

When the cowl bluntness is sufficiently big, the narrow longitudinal separation zones are combined into a common separation region at some distance from the cowl leading edge. This is manifested in the fall of the Stanton number on the cowl and wedge surfaces in zone *8* (Fig.7,*b*), in curvature of the surface stream lines on the wedge surface in front of the region *8* (Fig.7,*a*), and in decrease the shear stress in this region (decrease in shear stress is displayed qualitatively in Figure 7 by the color change from red to blue). However, this does not lead to the formation of global separation zone and blocking the channel. This can be explained by small thickness of the boundary layer and, correspondingly, by small size of the separation zone on the cowl. But at the chosen inlet height, the bow shock wave generated by the blunted leading edge of the cowl can reach the plate surface and cause global separation of the boundary layer on it (Fig. 7a). The separation zone, in turn, generates an intense shock wave, which interacts with the bow wave of the cowl. Thus, at large cowl bluntness, the flow is similar to the flow at large plate bluntness.

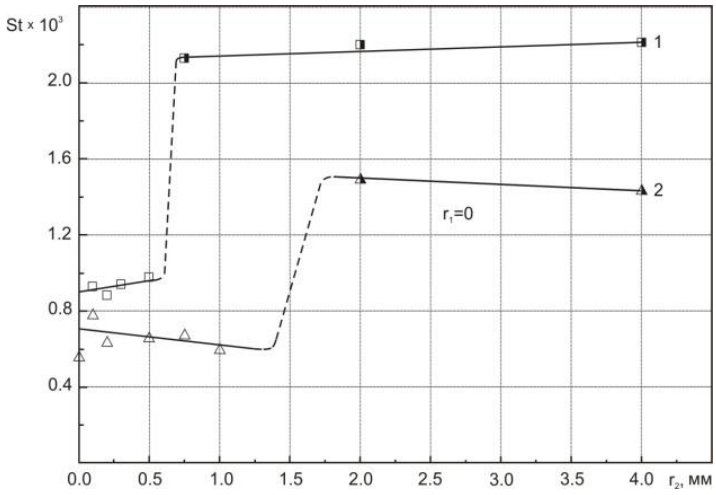

Fig 9. Influence of cowl bluntness on heat exchange on the cowl symmetry line in the cross section 1 at M_∞=5: *1* - $Re_{\infty L}=13\times10^6$, *2* - $Re_{\infty L}=23\times10^6$.

Fig. 8 displays influence of cowl blunting on heat exchange on its surface. The cowl bluntness radius causing inlet blockage at $Re_{\infty L}=23\times10^6$ ($r_2\approx1.5$ mm, $r_2/W_t\approx0.06$) is much larger than the analogous plate bluntness radius ($r_1\approx0.8$ mm, $r_1/W_t\approx0.032$). The reason for this is the difference in the mechanisms of the blunting impact on the inlet blockage: in the first case, the blockage is caused by the action of the cowl bow wave on the plate boundary layer, and in the second case, the blockage occurs due to the interaction of the wedges shocks with the plate entropy and boundary layers.

The decrease in the Reynolds number, as shown in Fig. 8, leads to decrease in the critical radius of the cowl bluntness, causing the inlet blockage: for $Re_{\infty L}=23\times10^6$, the blockage occurs when $r_2\approx1.5$ mm, and for $Re_{\infty L}=13\times10^6$ this occurs when $r_2\approx0.6$ mm.

5.3. Wedges bluntness radius r_3

Fig. 9 shows the Stanton number distribution along the plate symmetry line at two wedge bluntness radii: at $r_3=0$ the regular flow regime is established, and at $r_3=2$ mm, the inlet is locked. In the first case, two heat flux maxima are seen. The first maximum corresponds approximately to the intersection of the separation shocks, and the second one corresponds to the intersection of the wedges shocks. The point with the coordinates Z = 0, X = 235 mm, located on the plate near the first maximum, is used below as the indicator of the inlet blockage. With increasing r_3, the heat flux at this point varies only weakly as long as the regular flow in the inlet remains. When the inlet is locked, the Stanton number at this point increases sharply.

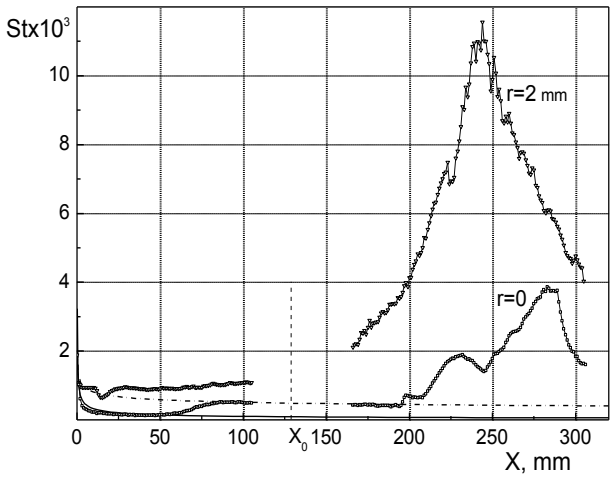

Fig 10. Stanton number distribution along the plate symmetry line at M_∞=5, $Re_{\infty L}$=23×10^6 and η = 4.

Fig. 10 demonstrates the effect of wedge blunting on the inlet blockage at different channel narrowing degrees η. With η = 4, the blockage occurs at relative wedge bluntness r_3/W_t=0.06 (r_3=1.5 mm), and with smaller narrowing degree η=3, the blockage is not observed even at the maximum wedge bluntness radius r_3=4 mm (r_3/W_t=0.12) (in Figure 10 and below, filled symbols correspond to the channel blockage). The following estimates are obtained for the value η_{ef}, corresponding the inlet blockage: at η=4, the inlet is locked with η_{ef}=4.53; at η=3, the bluntness radius r_3=4 mm corresponds to η_{ef}=3.28. This value is much smaller than in the previous case, which agrees with the fact that at η=3 the channel is not locked.

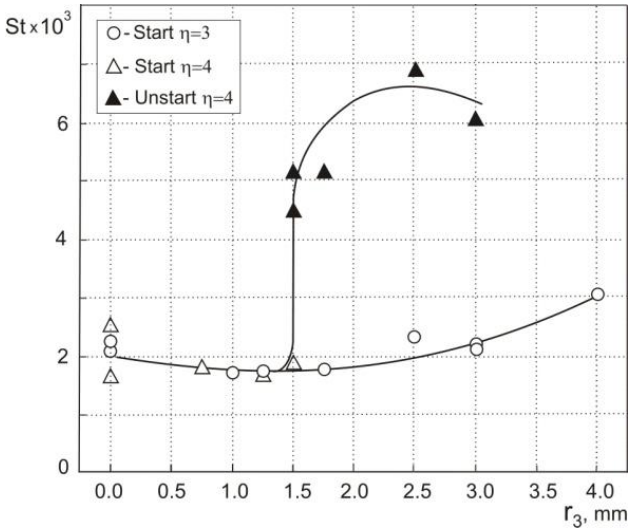

Fig 11. Influence of the wedge bluntness on the inlet blockage at M_∞=5 and $Re_{\infty L}$=22×10^6.

Fig. 11 displays the Reynolds number influence on the inlet blockage at various wedge bluntness. It reflects an unexpected fact: at the smaller Reynolds number $Re_{\infty L}$=8.5×10^6 (M_∞=5, η=3), there is a bluntness range r_3/W_t=0.06-0.11 (2<r_3<4 mm), in which are possible both the regular flow in the inlet and locking it. This result is discussed below.

With increasing the narrowing degree to η=4, the Reynolds number influence on the inlet flow is amplified (Figure 11,b): at $Re_{\infty L}$=22×10^6, the blockage is caused by the wedge relative bluntness 0.06 (r_3=1.5 mm, η_{ef}=4.53), and at $Re_{\infty L}$=13×10^6 it happens at r_3/W_t= 0.012 (r_3=0.3 mm, η_{ef}=4.28). The reason for such a strong influence of the Reynolds number on the inlet blockage is not clear.

At larger Mach number M_∞=8 and $Re_{\infty L}$=5.6×10^6, the inlet with narrowing degree η=4 is locked even with the sharp wedges (corresponding value of η_{ef}=4.37 for the laminar boundary layer). The inlet with smaller narrowing degree η=3 allows significant wedge blunting (Figure 12): in the case of

$Re_{\infty L}=5.6\times10^6$, the blockage occurs at $r_3/W_t=0.06$ ($r_3=2$ mm, $\eta_{ef}=3.55$), and in the case of $Re_{\infty L}=2.8\times10^6$ it happens at slightly less bluntness $r_3/W_t=0.052$ ($r_3=1.75$ mm, $\eta_{ef}=3.60$).

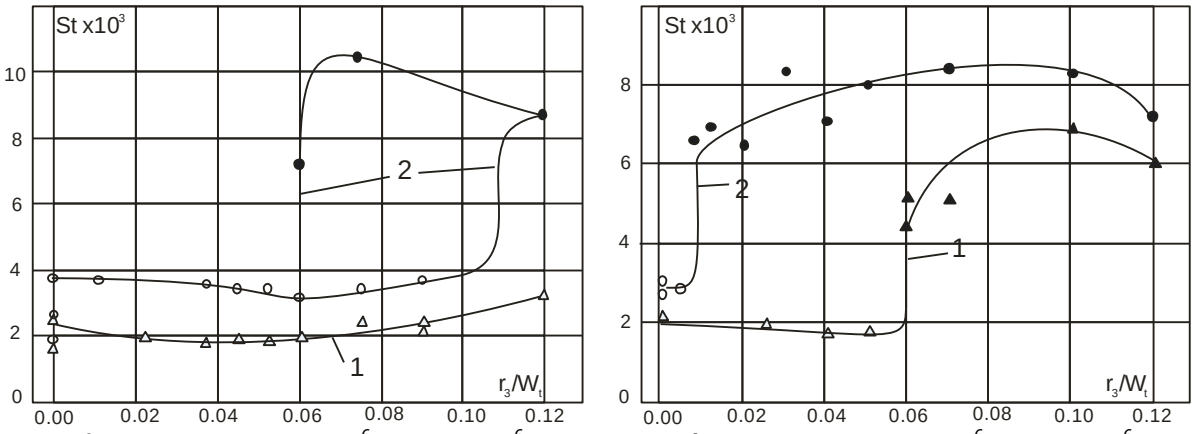

a) η=3, *1* – $Re_{\infty L}=22\times10^6$, *2* – $8.5–10^6$ *б*) η=4, *1* – $Re_{\infty L}=22\times10^6$, *2* – 13×10^6

Fig 12. Reynolds number influence on the inlet blockage at $M_\infty=5$ (*X*=235 mm, *Z*=0).

Fig. 12,*b* shows that at Mach number $M_\infty=8$, as at M_∞ = 5, there is a range of wedge bluntness, in which the flow regime is ambiguous. At $M_\infty=8$ and $Re_{\infty L}=2.8\times10^6$, the flow regime ambiguity is observed in the range $r_3/W_t\approx0.05$ - 0.11 ($1.75\le r_3\le3$ mm, $\eta_{ef}=3.60$ - 3.77). In the short duration (impulse) wind tunnel, such a phenomenon has apparently not been observed so far. From Fig. 12,*b* it is clear that beyond the branch point $r_3/W_t=0.05$ in the case of regular flow (open symbols), the same monotonic decrease of Stanton number continues, as before the branch point. This indicates that the observed phenomenon is not related directly to the laminar-turbulent transition of the boundary layer.

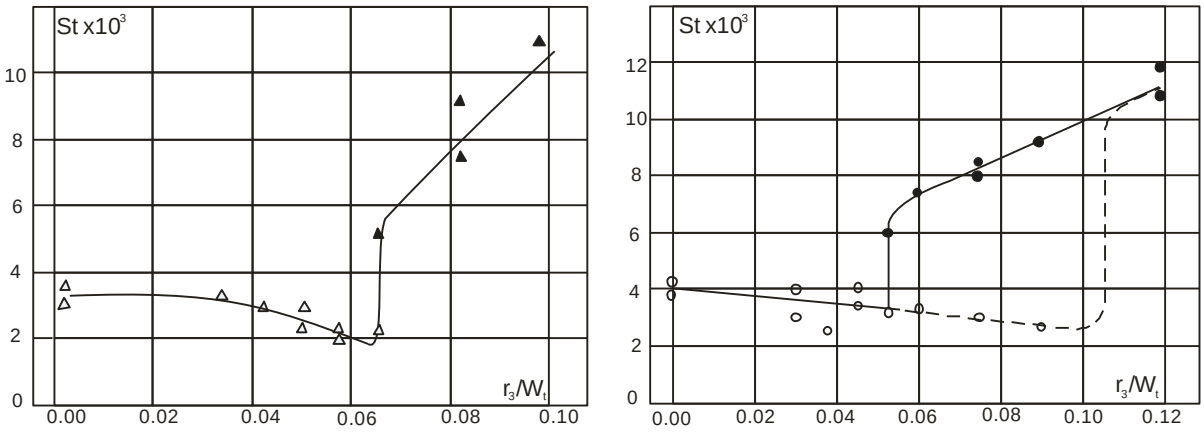

a) $Re_{\infty L}=5.6\times10^6$ *b*) $Re_{\infty L}=2.8\times10^6$

Fig 13. Reynolds number Influence on the channel blockage at $M_\infty=8$ and η=3.

Apparently, the reason for the ambiguity of the flow regime is the uncontrollable differences in the rate of pressure increase in the test chamber of the wind tunnel, due to small differences in the test conditions, for example, in the depth of gas evacuation from the test chamber. Another possible cause is the difference in the water vapour concentration in the air.

6. Conclusion

The study shows that even a small blunting of the inlet leading edges can lead to the inlet blockage. The effect of leading edge blunting is enhanced as the channel narrowing degree and the Mach number increases, and as the Reynolds number decreases.

At some combinations of inlet characteristics and flow parameters, the flow structure is ambiguous: it is possible both the starting and non-starting of the inlet.

References

1. Kantrowitz, A.: The formation and stability of normal shock waves in channel flows. NACA TN 1225. Mar. (1947)
2. Abramovich G.N.: Applied gas dynamics. Moscow (1969)
3. GurylevV.G., Ivanyushkin A.K., Piotrovich E.V.: Experimental investigation of Reynolds number Re_L influence on the inlet starting at high supersonic speeds. Uchenye zapiski TsAGI. V. 4, No.1, 33-44 (1973)
4. Staruhin V.P., Chevagin A.F.: Influence of leading edges blunting on the characteristics of inlets situated under wing. Uchenye zapiski TsAGI. V. 25, No.1-2, 89-100 (1994)
5. VanWie, D. M.: Scramjet inlets (Chapter 7). In: Curran,E.T. Murthy,S.N.B. (eds.) Scramjet Propulsion, Progress in Aeronautics and Astronautics. AIAA. V. 189. Pp. 447 - 511 (2000)
6. Goonko, Y. P., Latypov, A. F., Mazhul, I. I., Kharitonov, A. M., Yaroslavtsev, M. I., and Rostand, P.: Structure of flow over a hypersonic inlet with side compression wedges. AIAA Journal. 41, 3, 436 – 447 (2003)
7. Falempin, F., Goldfeld M., Nestoulia R., Sarov A.: Mach 2 – Mach 8 experimental evaluation of a simplified variable geometry air inlet. International Society for Air Breathing Engines.ISABE-2005-1251 (2005)
8. Falempin, F., and Wendling, F.: Experimental investigation of starting process for a variable geometry air inlet operating from Mach 2 to Mach 8. AIAA Paper 4513 (2006)
9. Häberle, J. and Gülhan, A.,: Investigation of the flow field of a 2D scram-jet inlet at Mach 7 with optional Boundary layer Bleed. AIAA Paper 5068 (2007)
10. Veillard Xavier, Tahir Rabi, Timofeev Evgeny, Mölder Sannu: Limiting contractions for starting simple ramp-type scramjet intakes with overboard spillage. Journal of Propulsion and Power. 24, 1042 - 1049 (2008)
11. Wagner J. L., Yuceil K. B.,. Valdivia A, Clemens N. T., and Dolling D. S.: Experimental investigation of unstart in an inlet/isolator model in Mach 5 flow. AIAA J. 47, 6, 1528 - 1542 (2009)
12. Mahapatra D. and Jagadeesh G.: Studies on unsteady shock interactions near a generic scramjet inlet. AIAA J. 47, 9, 2223 - 2231 (2009)
13. Throckmorton R., Schetz J. A., and Jacobsen L.S.: Experimental and computational investigation of a dynamic starting method for supersonic/hypersonic inlets. AIAA Paper. 2010-589 (2010)
14. Tan Hui-jun, Li Liu-gang, Wen Yu-fen, and Zhang Qi-fan: Experimental investigation of the unstart process of a generic hypersonic inlet. AIAA J. 49, 2, 279 – 285 (2011)
15. Borovoy V.Ya., Mosharov V.E., Radchenko V.N, Skuratov A.S, Struminskaya I.V.: Effect of leading edges blunting on the flow in the model air inlet. Izvestia RAN, Mekhanika Zhidkosti i Gasa. 4, 43-57 (2014)
16. Borovoy V.Ya., Egorov I.V., Mosharov V.E., Skuratov A.S., Struminskaya I.V. , Radchenko V.N.: Bluntness effect of gas-contracting wedges on the starting of a generic inlet. TsAGI Science Journal. 47, 3, 309-327 (2016)
17. Mosharov V.E., Radchenko V.N.: Measurement of heat flux fields in short-duration wind tunnels using luminescent temperature converters. Uchenye zapiski TsAGI. 28,1-2, 94-101 (2007)
18. Mosharov V.E., Radchenko V.N.: A new method for flow visualizing on the surface of aerodynamic models. Datchiki I sistemy. 5, 48 - 53 (2010)

19. Borovoy V.Ya., Egorov I.V., Mosharov V.E., Radchenko V.N, Skuratov A.S, Struminskaya I.V.: Interference of intersecting shocks with a flat-plate boundary layer in the presence of an entropy layer. Fluid Dynamics. 48, 5, 636-647 (2013)

20. Zheltovodov Alexander A. and Knight Doyle D.: Ideal-gas shock wave–turbulent boundary-layer interactions in supersonic flows and their modeling: three-dimensional interactions. In: Babinsky H., Harvey J.K. (eds.) Shock Wave-Boundary-Layer Interactions. Cambridge University Press, 202–258 (2011)